Inorganic Chemistry

Article

pubs.acs.org/IC

Wide-Band Excited $Y_6(WMo)_{0.5}O_{12}$:Eu Red Phosphor for White Light Emitting Diode: Structure Evolution, Photoluminescence Properties, and Energy Transfer Mechanisms Involved

Huaiyong Li,*[,†] Hyeon Mi Noh,[‡] Byung Kee Moon,[‡] Byung Chun Choi,[‡] Jung Hyun Jeong,*[,‡] Kiwan Jang,[§] Ho Sueb Lee,[§] and Soung Soo Yi[∥]

[†]Department of Materials Science and Engineering, Liaocheng University, Liaocheng 252059, P. R. China

[‡]Department of Physics, Pukyong National University, Busan 608-737, Korea

[§]Department of Physics, Changwon National University, Changwon 641-773, Korea

[∥]Department of Electronic Material Engineering, Silla University, Busan 617-736, Korea

Supporting Information

ABSTRACT: $Y_6(WMo)_{0.5}O_{12}$ activated with Eu^{3+} ions was investigated as a red-emitting conversion phosphor for white light emitting diodes (WLEDs). The phosphors were synthesized by calcining a citrate-complexation precursor at different temperatures. The photoluminescence properties of the phosphors and the energy transfer mechanisms involved were studied as a function of structure evolution. It was found that the host lattices were crystallized in a cubic or a hexagonal phase depending on the synthesis conditions. Although all the phosphors showed intensive red emission under an excitation of near-UV or blue light due to energy transfer from the host lattices to Eu^{3+} ions, the photoluminescence spectra and temporal decay features were found to vary significantly with the structure and crystallinity of the host lattice. The mechanisms of the energy transfer from the host lattices to Eu^{3+} ions and energy quenching among Eu^{3+} ions were discussed on the basis of structure evolution of the host lattice. Phosphors calcined at 800 and 1300 °C were suggested to be promising candidates for blue and near-UV light excited WLEDs, respectively.

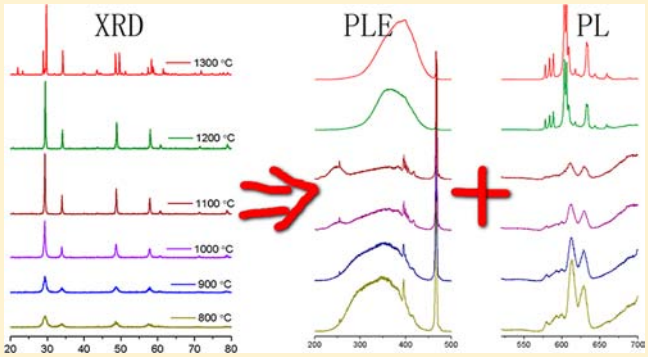

INTRODUCTION

Solid-state lighting achieved by light emitting diode (LED) chips and color conversion phosphors has many advantages over conventional light sources, such as being energy-saving, environmentally friendly, compact, portable, and easy to maintain, and therefore is a promising light source.[1,2] At present, the widely used commercial white light emitting diode (WLED) comprising a blue LED with a yellow phosphor ($Y_3Al_5O_{12}:Ce^{3+}$) has a low color rendering index because of the lack of red emission.[3−5] A solution to this problem is to introduce a red phosphor and use the combinations of near-UV/blue LED chips and trichromatic phosphors.[4−6] However, the commercial red phosphor ($Y_2O_2S:Eu^{3+}$) has some serious drawbacks in terms of low absorption efficiency of near-UV light in the range of 370−450 nm and poor stability under near-UV radiation.[7] Therefore investigations of red phosphors for use in WLEDs have attracted a great amount of interest.[8]

To be used for a WLED, the candidate red phosphor is desired to have a wide excitation band, which overlaps the emission wavelength of the LED chips. At the same time, the candidate is required to convert the excitation energy into efficient red emission.[2,4,5] According to these requirements, a great number of compounds have been suggested to be host lattices for red phosphors, among which molybdates and tungstates have received considerable attention because of their high stability and outstanding properties.[8−17] We focus our attention on molybdates containing MoO_6 groups[18−20] because they exhibit intensive and wide absorption of near-UV light at about 400 nm due to the charge transfer transition from O to Mo within the MoO_6 groups.[7,8,18−27] And furthermore the energy transfer from MoO_6 groups to Eu^{3+} ions doped is efficient.[18−27] It is known that there are energy migration and quenching processes among MoO_6 groups which compete with the energy transfer process, and consequently reduce the photoluminescent efficiency of the phosphor.[19−27] According to the literature, implanting WO_6 groups or introducing other lattice defects into the MoO_6 network could reduce the energy quenching among MoO_6 groups, and lead to an increase of the photoluminescent intensity.[18,28,29] In a previous work, we have reported the photoluminescence (PL) properties of Eu^{3+} ion-activated $Y_6W_xMo_{(1-x)}O_{12}$ red phosphor, which is a promising

Received: June 8, 2013
Published: September 16, 2013

   dx.doi.org/10.1021/ic401453e | Inorg. Chem. 2013, 52, 11210−11217

candidate for WLEDs.[20] However, the energy transfer and quenching behaviors within the phosphors, and their dependence on the structure of the host lattice as well as doping concentration of Eu^{3+} ions have not been well characterized and understood. It is known that these facts have a strong effect on the PL properties of the phosphors.

Because of these reasons, we performed an investigation on the PL properties of Eu^{3+} ion-activated $Y_6(WMo)_{0.5}O_{12}$. A citrate-complexation method was used to synthesize the precursor, and a modification of the calcination temperature was used to adjust the crystallinity of the host lattice. The crystallite morphology, crystalline structure, PL spectra, and temporal decay of the obtained phosphors were characterized. The competition between the energy transfer from the host lattices to Eu^{3+} ions and energy quenching in the host lattices was characterized as a function of structure. The energy quenching behavior of Eu^{3+} ions in different host lattices was also studied.

EXPERIMENTAL METHODS

Synthesis. The starting materials, $Y(NO_3)_3{\cdot}6H_2O$ (99.9%), $Eu(NO_3)_3{\cdot}5H_2O$ (99.9%), $(NH_4)_6Mo_7O_{24}{\cdot}4H_2O$ (99.98%), $(NH_4)_{10}H_2(W_2O_7)_6$ (99.99%), and citric acid (>99.5%), were obtained from Sigma-Aldrich, and used without further purification.

$Y_6(WMo)_{0.5}O_{12}$:Eu (YWMO:Eu) phosphors containing different doping concentrations of Eu^{3+} ions, namely 2.5, 5, 10, 15, 20, and 25 molar percent (mol %) of Y, were synthesized by using a citrate complexation method, and followed by calcination at different temperatures. In a typical procedure, for example, the synthesis of YWMO:Eu(2.5%), $Y(NO_3)_3{\cdot}6H_2O$ (11.70 mmol, 4.481 g), $Eu(NO_3)_3{\cdot}5H_2O$ (0.30 mmol, 0.128 g), and citric acid (24.0 mmol, 4.611 g) were dissolved in 30 mL of distilled water to form solution A. $(NH_4)_6Mo_7O_{24}{\cdot}4H_2O$ (0.143 mmol, 0.177 g), $(NH_4)_{10}H_2(W_2O_7)_6$ (0.083 mmol, 0.254 g) as well as citric acid (4.0 mmol, 0.768 g) were dissolved in 10 mL of distilled water to form solution B. Then solution B and 60 mL of ethanol were successively poured into solution A under vigorous stirring. The pH value of the mixture was finally adjusted to 2−3 by dilute $NH_3{\cdot}H_2O$ and HNO_3. After being stirred for 30 min, the mixture was water-bathed at 70 °C until a porous precursor jelly was formed. The precursor was successively heated at 200 °C for 4 h and precalcined at 700 °C for 4 h in air. After being finely ground, the powder was divided into six patches and calcined at different temperatures from 800 to 1300 °C with an interval of 100 °C for 4 h in air, respectively.

Characterization. Thermogravimetric/differential thermal analysis (TG/DTA) of the precursor was carried out on a TG-DTA 2020 from room temperature to 1100 °C at a heating rate of 10 °C min^{-1}. The morphologies of the phosphor were checked by field emission scanning electron microscope (FE-SEM) on a JSM-6700F at 15 kV. The compositional analysis was performed by energy dispersive X-ray spectroscopy (EDS) on the JSM-6700F. The structure of the host lattice and its evolution were examined by using powder X-ray diffraction (PXRD) measurements, which were carried out on a Philips X'Pert MPD X-ray diffraction system at 40 kV and 30 mA with Cu $K\alpha_1$ radiation (λ = 1.54056 Å) as incident beam. The diffraction patterns were scanned over 20°−80° (2θ) with a step length of 0.02° (2θ). The PL measurements were performed on a PTI fluorescence spectrophotometer equipped with a 60 W Xe-arc lamp as the excitation light source. The temporal decay of the PL was measured by the fluorescence spectrophotometer with a phosphorimeter attachment. All the measurements were performed at room temperature in air.

RESULTS AND DISCUSSION

Thermal Analysis, Morphology, Composition, and Structure Evolution. The thermal decomposition behavior of the precursor jelly is characterized by a TGA/DTA measurement in air. The TGA curve shown in Figure 1

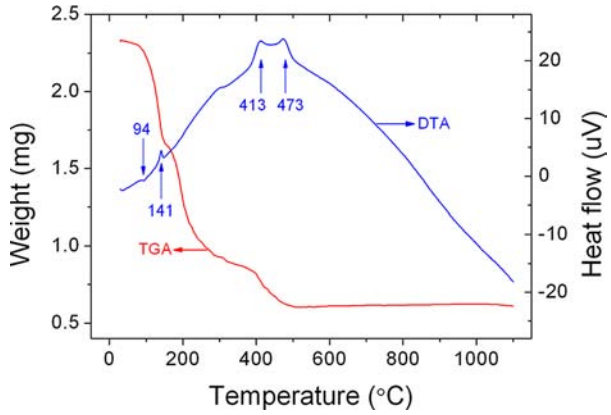

Figure 1. Thermal analysis data of the precursor jelly.

indicates that there are three stages of weight loss in the range of 25−500 °C. The first stage ranges from 25 to 140 °C with an endothermic pick at 94 °C in the DTA curve, which is related to the evaporation of free water and organic solvents. The subsequent stage starts with an exothermic peak at 141 °C in the DTA curve, up to 400 °C, corresponding to the initial decomposition of citric acid and nitrate, and removal of residual water. The third weight loss stage is in the 400−500 °C range accompanied by two strong exothermic peaks centered at 413 and 473 °C. This stage is assigned to the combustion of residual carbon and final decomposition of nitrate. Beyond 500 °C the weight is kept constant and no obvious endothermic or exothermic peak is observed, indicating a complete decomposition of the precursor.

Figure 2 shows the SEM microimages and EDS data of YWMO:Eu(2.5%) calcined at 800 to 1300 °C. As seen in the figure the obtained phosphors are aggregate particles. The particle size ranges from 100 to 300 nm in diameter, and increases gradually with the calcination temperature from 800 to 1300 °C. At the same time, the crystallinity is also enhanced with the calcination temperature. A morphology of sharp edge and smooth surface can be observed in the phosphors calcined at 1200 and 1300 °C, which indicates that the phosphors have good crystallinity. The EDS data confirms the presence of Y, Mo, W, O, and Eu elements in the phosphors. The constituent ratio of (Y+Eu):W:Mo:O is determined to be 30.62:1.83:2.35:65.24, which agrees approximately with the theoretical ratio of 6:0.5:0.5:12.

The PXRD patterns shown in Figure 3 indicate that the crystal structure and crystallinity of YWMO:Eu(2.5%) depend strongly on the calcination temperature. The host lattice is in a cubic phase when the calcination temperature is below 1200 °C, while it is in a hexagonal phase at 1300 °C. The diffraction patterns of the cubic and hexagonal phases can be indexed to JCPDS cards #35-0174 and #20-1420, respectively.[30,31] The PXRD patterns also suggest that the crystallinity of the cubic phase varies systematically with calcination temperature. The diffraction peaks of the phosphor calcined at 800 °C show a broad and weak character because of the lack of long-range order in the host lattice, and they become narrow and intensive with an increment in the calcination temperature. For example, the full width at half-maximum (fwhm) of the (111) peak in the cubic phase decreases gradually from 0.741° to 0.209° (2θ) when the calcination temperature increases from 800 to 1200 °C.

dx.doi.org/10.1021/ic401453e | Inorg. Chem. 2013, 52, 11210−11217

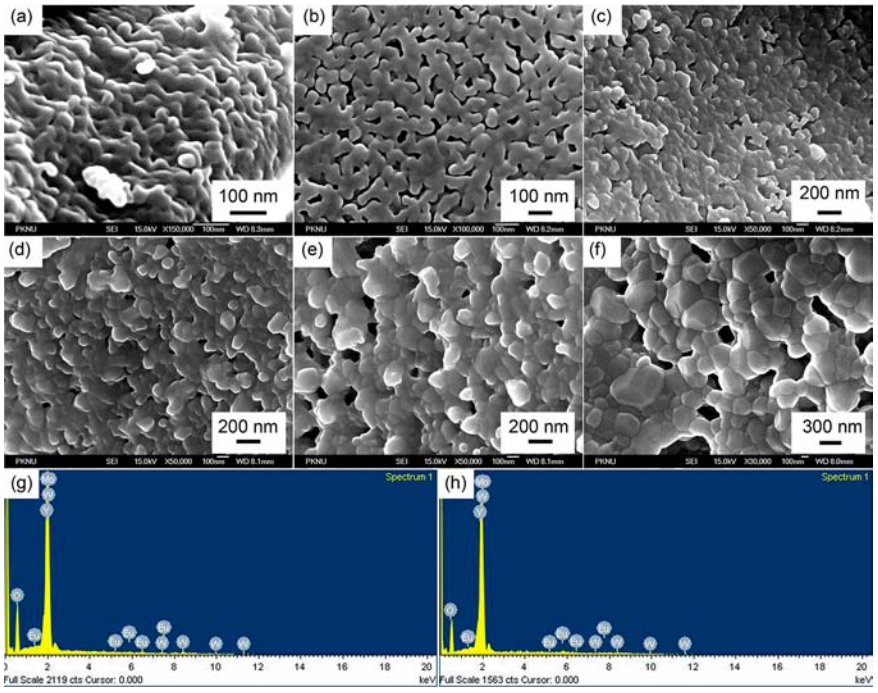

Figure 2. SEM microimages and EDS data of YWMO:Eu(2.5%) calcined at different temperatures: (a) and (g) 800 °C, (b) 900 °C, (c) 1000 °C, (d) 1100 °C, (e) 1200 °C, (f) and (h) 1300 °C.

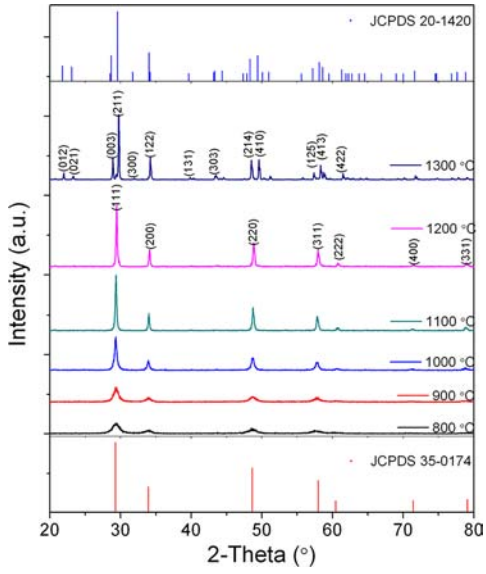

Figure 3. PXRD patterns of YWMO:Eu(2.5%) calcined at different temperatures and JCPDS cards of Y_6WO_{12} in hexagonal and cubic phases.

PL Excitation Spectra and Energy Transfer from Host Lattice to Eu^{3+} Ions. Figure 4 shows the PL excitation spectra of YWMO:Eu(2.5%) calcined at different temperatures by monitoring the $^5D_0$-$^7F_2$ emission of Eu^{3+} ions (at 606 nm for samples calcined at 1200 and 1300 °C, or at 613 nm for the others). As expected, all the spectra contain a series of characteristic excitations due to Eu^{3+} ion f-f transitions, such as the $^7F_0$-$^5L_6$ transition at 396 nm and the $^7F_0$-$^5D_2$ transition at 467 nm. The intensities of these excitations are hardly changed with the calcination temperature. Additionally, broad excitation bands that lie in the UV and blue spectral region are also observed. It is seen that the excitation bands differ remarkably from each other in both profile and intensity. By using a Gaussian analysis, we decompose the excitation bands into several components, namely, A, B, C, and D as shown in Figure 4. Band A resides in the 200−300 nm range with a maximum at 250 nm, and is identified as the charge transfer (CT) transition from O^{2-}(2p-orbitals) to Eu^{3+}(4f-orbitals). Band B, situated in the 250−350 nm range with a maximum at about 300 nm, is generally ascribed to the CT transition from O-2p orbitals to W-5d orbitals within WO_6 groups,[18,20,25] C and D in the near-UV region to the excitation of MoO_6 groups, from O-2p orbitals to Mo-4d orbitals.[18,20,25] Similar bands have been observed in other tungstate and molybdate compounds, and attributed to the excitation of $W(Mo)O_x$ groups in the host lattices. However, it is observed that the intensity of the $W(Mo)O_x$ excitation generally increases with the crystallinity of the host lattices because of less energy dissipation, such as in R_2MoO_6 (R = La, Gd, Y, and Lu),[28,29] and $Na_5R(MoO_4)_4$ (R = La, Gd, and Y) systems.[32] In our cases, the intensities of B, C, and D bands decrease with the crystallinity of the host lattices from YWMO:Eu-800 to YWMO:Eu-1100. On this basis, we ascribe the excitation bands to the disorder of lattice and $W(Mo)O_6$ for samples calcined from 800 to 1100 °C, and to $W(Mo)O_6$ for those calcined 1200 and 1300 °C. It is established that surface states, defects, and disorder of the lattice of a semiconductor might induce PL, whose intensity depends on the defect states.[33−38] The PXRD patterns of the samples calcined from 800 to 1100 °C indicate that the disorder of lattice decreases with the calcination temperature, and therefore is proportional to the PL intensity. For this reason we suggest the above-mentioned ascription. According to the excitation spectra, the excitation and energy transfer processes involved are schematically plotted in Figure 5. The presence of the excitation bands due to WO_6 and MoO_6 groups indicate that there is energy transfer from the host lattices to Eu^{3+} ions. In other words, the Eu^{3+} ion dopant could be activated through two channels, namely, sensitizing MoO_6 or

dx.doi.org/10.1021/ic401453e | Inorg. Chem. 2013, 52, 11210−11217

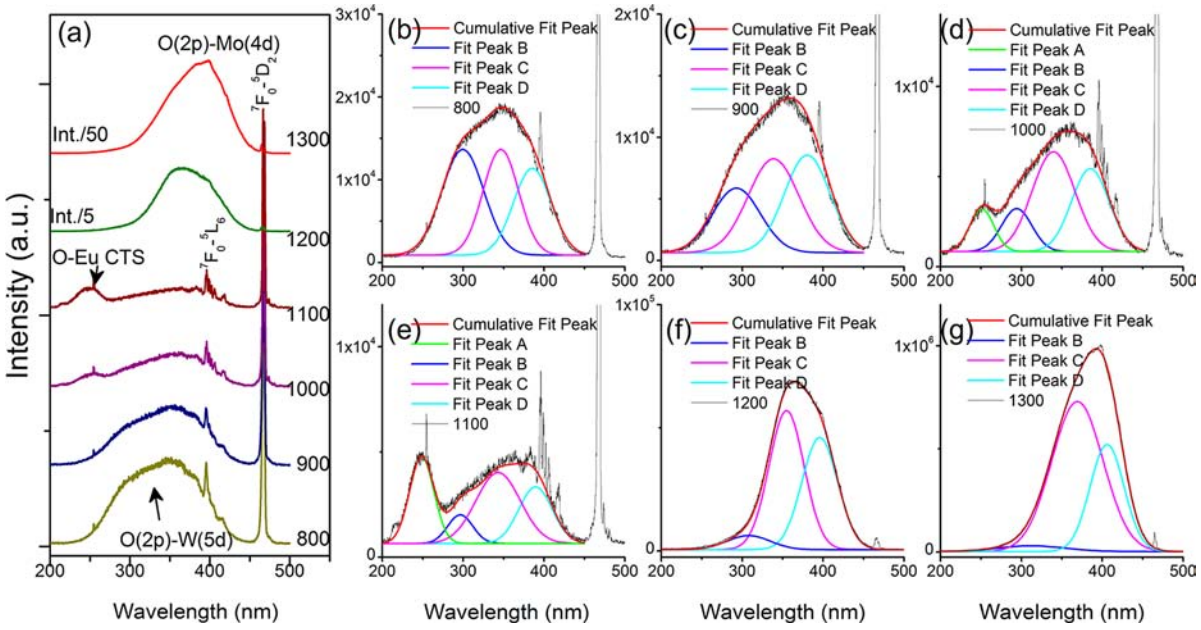

Figure 4. (a) PL excitation spectra of YWMO:Eu(2.5%) phosphors calcined at different temperatures, and (b)−(g) Gaussian analysis of the excitation bands.

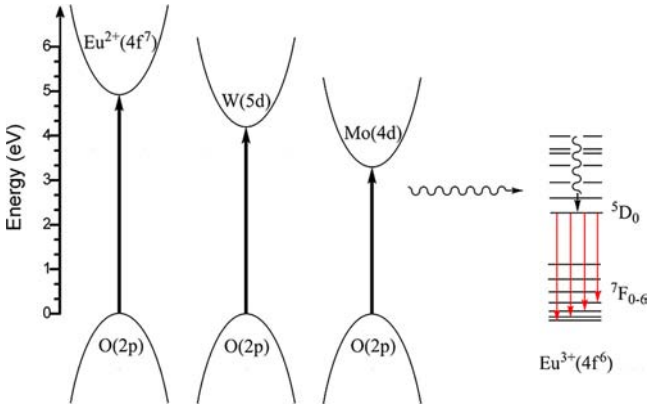

Figure 5. Excitations of Eu−O CTB, WO_6 and MoO_6 groups, and energy transfer to Eu^{3+} ions.

WO_6 groups in the host lattices and then transferring the energy from the host lattices to Eu^{3+} ions, or sensitizing Eu^{3+} ions directly via the f-f transitions or CT transitions. It should be noted that the excitations due to MoO_6 and WO_6 groups are spin and parity allowed, and therefore they usually are more efficient than the excitation of Eu^{3+} ions via f-f transitions. This rule works well on the samples calcined at 1200 and 1300 °C. In the excitation spectra of these two samples, the excitations due to the host lattices are significantly more intensive than those due to the f-f excitations of Eu^{3+} ions. While for the others, the excitation due to the host lattice is relatively weak with respect to the intrinsic excitation of Eu^{3+} ions. This implies that multiphonon assisted energy dissipation prevails in the samples calcined at low temperatures, and consequently a great amount of excitation energy is dissipated before it can be trapped by Eu^{3+} ions.

PL Emission Spectra and Temporal Decay. The emission spectra of the as-prepared phosphors were examined by sensitizing Eu^{3+} ion dopant as well as the host lattices, and interesting results are observed. The spectra shown in Figure 6a are obtained by exciting Eu^{3+} ions directly with blue light. Quite

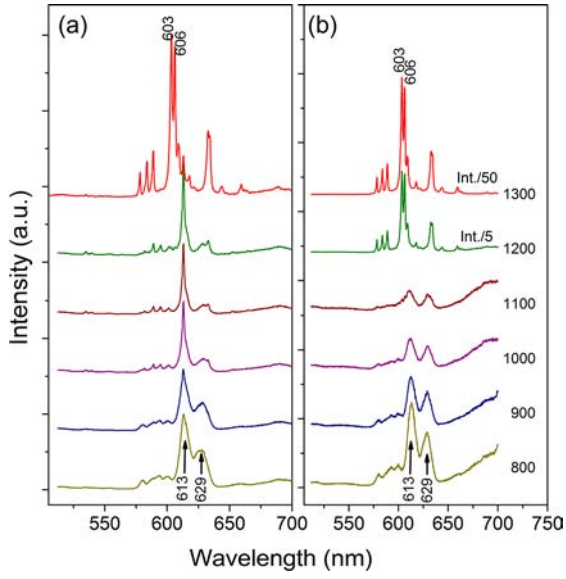

Figure 6. PL emission spectra of YWMO:Eu(2.5%) phosphors calcined at different temperatures. The spectra were obtained after exciting the phosphors into (a) the f-f transition of Eu^{3+} ions, and (b) the host lattices.

sharp and distinct peaks corresponding to the $^5D_0$-$^7F_0$ (578 nm), -$^7F_1$(584 nm, 589 and 603 nm), -$^7F_2$(606 nm, 609 nm, 618 nm, 633 nm and 634 nm), -$^7F_3$(640−670 nm), -$^7F_4$(680−700 nm) transitions are observed of YWMO:Eu phosphors calcined at 1300 °C.[18,39] The presence of these emission lines is in accordance with the C_1 symmetry of the site that is occupied by Eu^{3+}(Y^{3+}) ions in the hexagonal lattice.[18,39,40] Under this symmetry, the degeneracy of the ^7F_J energy levels is totally removed, and consequently there are 1, 3, and 5 emission lines corresponding to the transitions from the $^5D_0$ level to the ^7F_J (J = 0, 1, and 2) sublevels could be observed.

The emission spectra of the cubic phase (samples calcined under 800−1200 °C) are similar to those of Gd_6WO_{12} and

dx.doi.org/10.1021/ic401453e | Inorg. Chem. 2013, 52, 11210−11217

Y_6WO_{12},[11,12] but significantly differ from that of the hexagonal YWMO:Eu. Although the spectra are still dominated by the $^5D_0$-$^7F_2$ transitions, the main emission shifts to 613 nm and 629 nm. The emissions from the $^5D_0$ level to other ^7F_J (J = 0, 1, 3, 4) levels are much weaker. It is well-known that the $^5D_0$-$^7F_2$ transition is of electric dipole type and is highly sensitive to site symmetry, while the $^5D_0$-$^7F_1$ magnetic dipole transition is not. Therefore the intensity ratio of $^5D_0$-$^7F_2$ to $^5D_0$-$^7F_1$ emissions is commonly used as a measurement that examines the deviation of a site from inverse symmetry. In our cases, the intensity ratio of the cubic phase (including samples calcined at 800−1200 °C) is far larger than that of the hexagonal phase (sample calcined at 1300 °C). This indicates that the symmetries of Eu^{3+} ion sites in the two phases are different, and the sites in the cubic phase derived far from inverse symmetry than those in the hexagonal phase. Furthermore, obviously broadened emission peaks are observed from the phosphors calcined at low temperatures, such as 800 and 900 °C, which suggests that the homogeneity of Eu^{3+} ion sites is poor because of a lack of the short-range order.

The emission spectra shown in Figure 6b are obtained from sensitizing the host lattices with near-UV light. In the case of the hexagonal phase, namely, YWMO:Eu(2.5%)-1300, the host lattice-sensitized spectrum is identical to the Eu^{3+} ion-sensitized one in the profile. On the other hand, the spectra of the cubic phase shown in Figure 6a and 6b differ significantly from each other. In Figure 6a the profiles of the emission peaks become sharp and intensive from YWMO:Eu(2.5%)-800 to YWMO:Eu(2.5%)-1100, while a converse trend is shown in Figure 6b. In addition, the emission spectra of YWMO:Eu(2.5%)-1200 deserve special attention. It is observed that the spectrum shows a sudden change in the profile when the excitation channel is altered. This leads naturally to the conclusion that Eu^{3+} ions in YWMO:Eu(2.5%)-1200 having different local environments and symmetries are activated.[41] One corresponds to the cubic phase (see Figure 6a), and the other corresponds to the hexagonal phase (see Figure 6b). However it is confirmed from the XRD pattern that the host lattice of YWMO:Eu(2.5%)-1200 is in the cubic phase, and no distinguishable diffraction peaks due to the hexagonal phase are observed. We would like to propose the assumption that the host lattice is still ordered over the long-range, while a fraction of the cation polyhedra is distorted in the local symmetry.[33] This local distortion cannot be visualized in the PXRD patterns while it can be probed by Eu^{3+} ion luminescence.

The nonradiative energy transfer processes among Eu^{3+} ions as well as from MoO_6 groups to Eu^{3+} ions are considered to be responsible for the above-mentioned phenomenon. Since the spectra shown in Figure 6a are obtained from sensitizing Eu^{3+} ions directly, a change in the coordination environment and the symmetry of the Y(Eu) sites has an immediate effect on the emission spectra. The PXRD patterns confirm that the samples obtained at low calcination temperatures are of poor crystallinity. It is reasonable to expect that the host lattices of the phosphors calcined at low temperatures lack long-range order, and the symmetry of the site therein is distorted and nonhomogenerous to a certain degree. Under this condition, the emission spectra of Eu^{3+} ions show a broad characteristic, which is similar to those observed in glass.[42,43] As the crystallinity and long-range order of the host lattice increase with the calcination temperature, the site distortion reduces, and the site homogeneity enhances. Characteristic emissions with a line profile are observed. In Figure 6b, MoO_6 groups in the host lattices are sensitized. It is reported that there are competitive nonradiative energy transfer processes undergoing after the MoO_6 groups are excited. One is energy transfer from MoO_6 groups to dopant Eu^{3+} ions, which benefits the luminescent efficiency. The other is the multiphonon relaxation of the excited MoO_6 groups, which quenches the luminescence.[19,20,24,25] In the samples calcined at low temperatures, the couple interaction between excited MoO_6 groups and the host lattice around it is weak because of the lack of long-range order. An increment in the calcination temperature from YWMO:Eu(2.5%)-800 to YWMO:Eu(2.5%)-1100 facilitates the long-range order in the lattice. Therefore more and more excited energy is dissipated through the host lattice and attributed to the enhanced couple interaction. The sudden change in the spectra of YWMO:Eu(2.5%)-1200 indicates that a structure transition from cubic to hexagonal starts, and so does the symmetry of Y(Eu) sites.

The temporal decay property of the $^5D_0$ energy level of Eu^{3+} ions is checked by sensitizing the phosphors through both channels. The data shown in Figure 7 is obtained after exciting

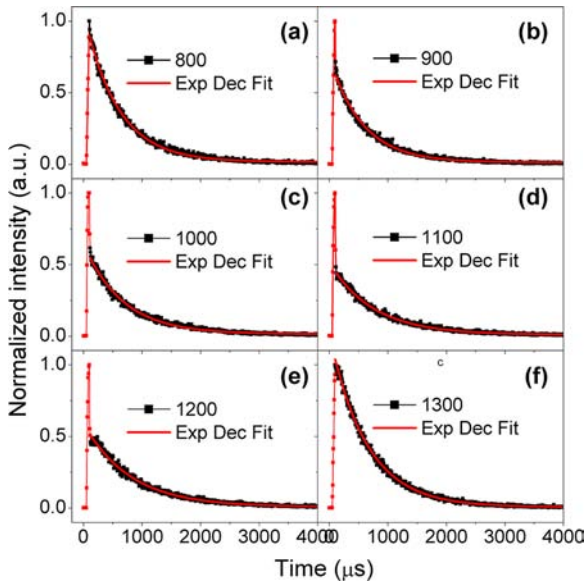

Figure 7. Temporal decays of the PL emissions of YWMO:Eu(2.5%) calcined at different temperatures. The phosphors were excited into the f-f transition of Eu^{3+} ions.

Eu^{3+} ions into the $^5D_2$ energy level. For the phosphors calcined at 800 and 1300 °C, the decay data could be fitted to a single-exponential function

$$I_t = I_0 \exp(-t/\tau) \quad (1)$$

where I_t and I_0 are the intensity at time t and 0, respectively, and τ is the lifetime. Whereas for those calcined at 900−1200 °C, the decay curves consist of two components: a very fast decay with a growing decay rate at the beginning, and a characteristic exponential component following, which could be fitted well to eq 1. The data after exciting MoO_6 groups is shown in Figure 8, and all the curves could be fitted to eq 1. The determined luminescence lifetimes are plotted in Figure 9.

Concentration Quenching and Energy Transfer among Eu^{3+} Ions. The color purities of the PL emissions are commonly characterized by the Commission Internationale de l'Eclairage (CIE) coordinates (x, y). The calculated values of

dx.doi.org/10.1021/ic401453e | Inorg. Chem. 2013, 52, 11210−11217

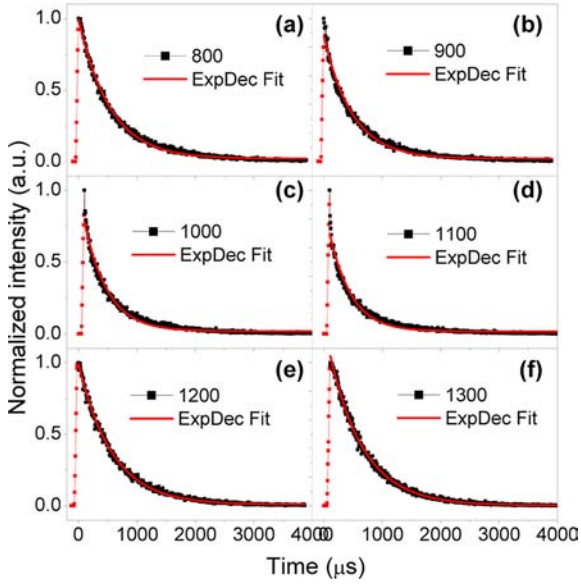

Figure 8. Temporal decays of the PL emissions of YWMO:Eu(2.5%) calcined at different temperatures. The phosphors were excited into the host lattices.

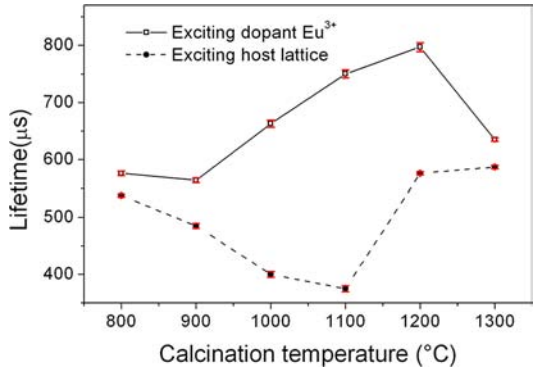

Figure 9. Lifetimes of the $^5D_0$-$^7F_2$ emission of Eu^{3+} ions in YWMO:Eu(2.5%) phosphors as a function of calcination temperature.

YWMO:Eu(2.5%) phosphors calcined at different temperatures are listed in Table 1. One may noticed that YWMO:Eu(2.5%)

Table 1. CIE Coordinates (*x*, *y*) of the Emission Spectra of YWMO:Eu(2.5%) Phosphors Shown in Figure 6

calcination temperature	Eu^{3+} ion-activated	host lattice-activated
800	(0.628, 0.367)	(0.613, 0.380)
900	(0.619, 0.375)	(0.596, 0.395)
1000	(0.598, 0.392)	(0.570, 0.418)
1100	(0.586, 0.403)	(0.548, 0.437)
1200	(0.592, 0.398)	(0.621, 0.376)
1300	(0.617, 0.379)	(0.632, 0.367)

phosphors calcined at 800 and 1300 °C show the most intensive red-luminescence under the excitation of blue (at 467 nm) and near-UV (at 399 nm) light, respectively, and therefore they are of applicative importance as color conversion phosphors for solid state lighting based on blue or near-VU LED chips. Therefore, the dependence of the PL properties and the interaction among Eu^{3+} ions on the doping concentration was studied further. The PL emission spectra of YWMO:Eu-800 and YWMO:Eu-1300 containing different Eu^{3+} ion concentrations (from 2.5 mol % to 25 mol %) are shown in the Supporting Information, Figures S1 and S2. It is observed that there is not an obvious difference in the profile of the emissions spectra. The integral intensities of the PL emissions of YWMO:Eu-800 and YWMO:Eu-1300 phosphors are plotted as a function of Eu^{3+} ion concentration in Figure 10.

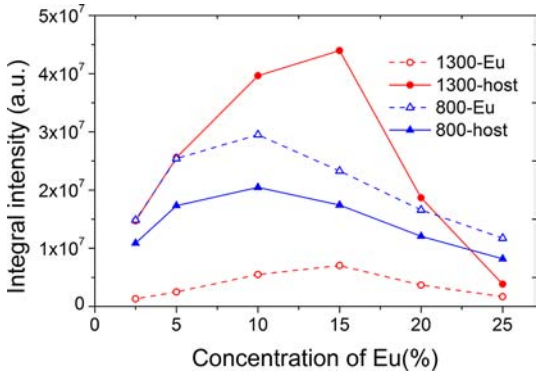

Figure 10. Integral intensities of the PL emission of YWMO:Eu phosphors calcined at 1300 and 800 °C as a function of Eu^{3+} ion concentration. The phosphors were excited into the host lattices as well as the f-f transition of Eu^{3+} ions.

It is well-known that there is generally a competition between radiative and nonradiative relaxations in Eu^{3+} ion-activated phosphors. If the content of Eu^{3+} ions reaches a critical value, the excitation energy can be lost via energy transfer process between Eu^{3+} ions by an exchange interaction,[44] and the luminescent efficiency is reduced. This is the so-called concentration quenching. Therefore the critical content of Eu^{3+} ions is an important parameter that determines the luminescent efficiency of a phosphor. According to Figure 10, the quenching concentrations of Eu^{3+} ions are determined to be about 10 mol % in YWMO:Eu-800 and 15 mol % in YWMO:Eu-1300. Since the concentration quenching of Eu^{3+} ions results from the energy transfer process, the decay time of the emission is reduced when the concentration quenching happens. Figures 11 and 12 show the emission decay profiles and lifetimes of YWMO:Eu-800 and YWMO:Eu-1300 as a function of Eu^{3+} ion concentration, respectively. In both hosts an obvious acceleration in the decay with Eu^{3+} ion concentration could be observed. It is also observed that the decay of Eu^{3+} emission is more sensitive to Eu^{3+} concentration in YWMO:Eu-800 series with respect to YWMO:Eu-1300 series. The decay of YWMO:Eu-1300 series accelerates slowly from 2.5 mol % to 20 mol % with a gradual decline in lifetime from about 600 to 500 μs, while for YWMO:Eu-800 samples, a fast acceleration starts from about 5.0 mol % and after that the lifetime of the Eu^{3+} ion emission decreases rapidly.

CONCLUSIONS

In this work, the PL properties of $Y_6(WMo)_{0.5}O_{12}$:Eu and the energy transfer mechanism involved were investigated in terms of the structure and crystallinity of the host lattice. It was revealed that the host lattice crystallized in a cubic phase at 800−1200 °C and in a hexagonal phase at 1300 °C. The obtained phosphors showed intensive absorption of near-UV light in the range of 300−420 nm and of blue light around 467 nm. The energy transfer from the host lattices to Eu^{3+} ions in the hexagonal phase was found to be more efficient than that in

dx.doi.org/10.1021/ic401453e | Inorg. Chem. 2013, 52, 11210−11217

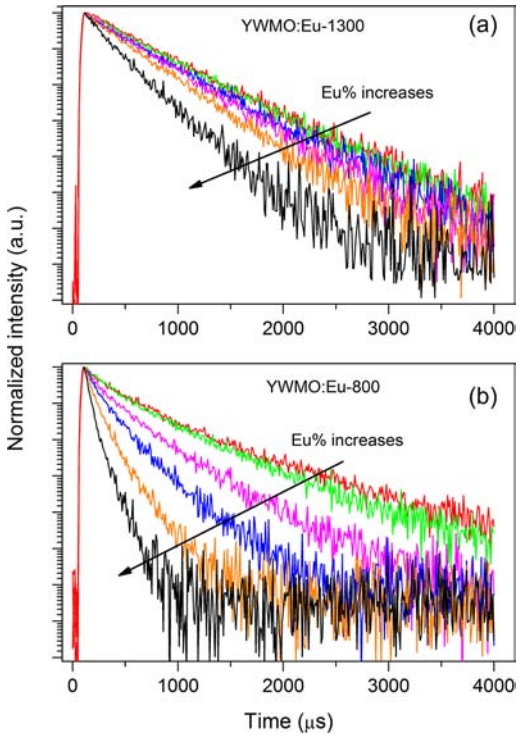

Figure 11. Temporal decays of the PL emissions of YWMO:Eu phosphors calcined at (a) 1300, and (b) 800 °C as a function of Eu^{3+} ion concentration.

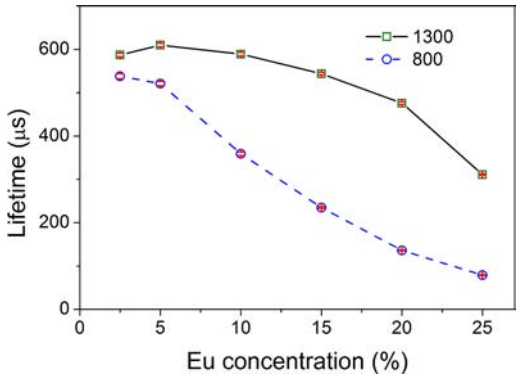

Figure 12. Lifetimes of the $^5D_0$-$^7F_2$ emission of Eu^{3+} ions in YWMO:Eu phosphors calcined at 1300 and 800 °C as a function of Eu^{3+} ion concentration.

the cubic phase because of less energy quenching. As a result, the hexagonal phase showed high photoluminescent efficiency under near-UV excitation, while the cubic phase was thought to be more suitable for blue chip-based WLEDs. The color purity of the PL emission and the quenching concentration of Eu^{3+} ions were also evaluated. It was observed that emissions of YWMO:Eu-800 and YWMO:Eu-1300 had a high color purity, and their quenching concentrations were determined to be 10 mol % and 15 mol %, respectively.

■ ASSOCIATED CONTENT

Ⓢ Supporting Information

Further details are given in Figures S1 to S2. This material is available free of charge via the Internet at http://pubs.acs.org.

■ AUTHOR INFORMATION

Corresponding Authors

*E-mail: huaiyong.lee@gmail.com (H.L.).

*E-mail: jhjeong@pknu.ac.kr (J.H.J.). Fax: +82-51-629-5549.

Notes

The authors declare no competing financial interest.

■ ACKNOWLEDGMENTS

This research was supported by Basic Science Research Program through the National Research Foundation of Korea (NRF) funded by the Ministry of Education, Science and Technology (No.2010-0022540 and 2012R1A1A2003979). A $Y_6(WMo)_{0.5}O_{12}$:Eu phosphor was supplied by the Display and Lighting Phosphor Bank at Pukyong National University.

■ REFERENCES

(1) Bergh, A.; Craford, G.; Duggal, A.; Haitz, R. *Phys. Today* **2001**, *54*, 42−47.

(2) Schubert, E. F.; Kim, J. K.; Luo, H.; Xi, J.-Q. *Rep. Prog. Phys.* **2006**, *69*, 3069.

(3) Yamada, M.; Naitou, T.; Izuno, K.; Tamaki, H.; Murazaki, Y.; Kameshima, M.; Mukai, T. *Jpn. J. Appl. Phys.* **2003**, *42*, L20.

(4) Silver, J.; Withnall, R. Color Conversion Phosphors for LEDS. In *Luminescent Materials and Applications*; Kitai, A., Ed.; John Wiley & Sons, Ltd: Chichester, U.K., 2008; pp 75−109.

(5) Justel, T. Luminescent Materials for Phosphor-Converted LEDs. In *Luminescence From Theory to Applications*; Ronda, C., Ed.; Wiley-VCH Verlag GmbH & Co. KGaA: Weinheim, Germany, 2008; pp 179−190.

(6) Schubert, E. F.; Kim, J. K. *Science* **2005**, *308*, 1274−1278.

(7) Yen, W. M.; Weber, M. J. *Inorganic Phosphors: Compositions, Preparation and Optical Properties*; CRC Press: Boca Raton, FL, 2004.

(8) Ye, S.; Xiao, F.; Pan, Y. X.; Ma, Y. Y.; Zhang, Q. Y. *Mater. Sci. Eng., R* **2010**, *71*, 1−34.

(9) Kumar, A.; Kumar, J. *J. Mater. Chem.* **2011**, *21*, 3788−3795.

(10) Raju, G. S. R.; Pavitra, E.; Ko, Y. H.; Yu, J. S. *J. Mater. Chem.* **2012**, *22*, 15562−15569.

(11) Zheng, Y.; You, H.; Liu, K.; Song, Y.; Jia, G.; Huang, Y.; Yang, M.; Zhang, L.; Ning, G. *CrystEngComm* **2011**, *13*, 3001−3007.

(12) Tian, Y.; Chen, B.; Hua, R.; Zhong, H.; Cheng, L.; Sun, J.; Lu, W.; Wan, J. *Phys. B* **2009**, *404*, 3598−3601.

(13) Longo, V. M.; Cavalcante, L. c. S.; Paris, E. C.; Sczancoski, J. l. C.; Pizani, P. S.; Li, M. S.; Andrés, J.; Longo, E.; Varela, J. A. *J. Phys. Chem. C* **2011**, *115*, 5207−5219.

(14) Marques, V. S.; Cavalcante, L. S.; Sczancoski, J. C.; Alcântara, A. F. P.; Orlandi, M. O.; Moraes, E.; Longo, E.; Varela, J. A.; Siu, Li, M.; Santos, M. R. M. C. *Cryst. Growth Des.* **2010**, *10*, 4752−4768.

(15) Sczancoski, J. C.; Bomio, M. D. R.; Cavalcante, L. S.; Joya, M. R.; Pizani, P. S.; Varela, J. A.; Longo, E.; Li, M. S.; Andrés, J. A. *J. Phys. Chem. C* **2009**, *113*, 5812−5822.

(16) Deng, K.; Gong, T.; Chen, Y.; Duan, C.; Yin, M. *Opt. Lett.* **2011**, *36*, 4470−4472.

(17) Dutta, P. S.; Khanna, A. *ECS J. Solid State Sci. Technol.* **2013**, *2*, R3153−R3167.

(18) Li, H.; Yang, H. K.; Moon, B. K.; Choi, B. C.; Jeong, J. H.; Jang, K.; Lee, H. S.; Yi, S. S. *Inorg. Chem.* **2011**, *50*, 12522−12530.

(19) Li, H.; Yang, H. K.; Moon, B. K.; Choi, B. C.; Jeong, J. H.; Jang, K.; Lee, H. S.; Yi, S. S. *J. Alloys Compd.* **2011**, *509*, 8788−8793.

(20) Li, H.; Yang, H. K.; Moon, B. K.; Choi, B. C.; Jeong, J. H.; Jang, K.; Lee, H. S.; Yi, S. S. *J. Mater. Chem.* **2011**, *21*, 4531−4537.

(21) Vaidyanathan, S.; Jeon, D. Y. *Int. J. Appl. Ceram. Technol.* **2009**, *6*, 453−458.

(22) Sivakumar, V.; Varadaraju, U. V. *J. Solid State Chem.* **2008**, *181*, 3344−3351.

(23) Sivakumar, V.; Varadaraju, U. V. *J. Electrochem. Soc.* **2007**, *154*, J28−J31.

(24) Sivakumar, V.; Varadaraju, U. V. *Electrochem. Solid-State Lett.* **2006**, *9*, H35−H38.
(25) Ye, S.; Wang, C. H.; Liu, Z. S.; Lu, J.; Jing, X. P. *Appl. Phys. B: Laser Opt.* **2008**, *91*, 551−557.
(26) Ye, S.; Wang, C. H.; Jing, X. P. *J. Electrochem. Soc.* **2008**, *155*, J148−J151.
(27) Ye, S.; Li, Y.; Yu, D.; Yang, Z.; Zhang, Q. *J. Appl. Phys.* **2011**, *110*, 013517−013515.
(28) Li, H.; Yang, H. K.; Jeong, J. H.; Jang, K.; Lee, H. S.; Yi, S. S. *Mater. Res. Bull.* **2011**, *46*, 1352−1358.
(29) Li, H.; Zhang, S.; Zhou, S.; Cao, X.; Zheng, Y. *J. Phys. Chem. C* **2009**, *113*, 13115−13120.
(30) Aitken, E. A.; Bartram, S. F.; Juenke, E. F. *Inorg. Chem.* **1964**, *3*, 949−954.
(31) Fournier, J. P.; Fournier, J.; Kohlmuller, R. *Bull. Soc. Chim. Fr.* **1970**, *12*, 4277−4279.
(32) Guo, C.; Gao, F.; Xu, Y.; Liang, L.; Shi, F. G.; Yan, B. *J. Phys. D: Appl. Phys.* **2009**, *42*, 095407.
(33) Campos, A. B.; Simoes, A. Z.; Longo, E.; Varela, J. A.; Longo, V. M.; de Figueiredo, A. T.; De Vicente, F. S.; Hernandes, A. C. *Appl. Phys. Lett.* **2007**, *91*, 051923−051923.
(34) Longo, V. M.; das Graca Sampaio Costa, M.; Zirpole Simoes, A.; Rosa, I. L. V.; Santos, C. O. P.; Andres, J.; Longo, E.; Varela, J. A. *Phys. Chem. Chem. Phys.* **2010**, *12*, 7566−7579.
(35) Lu, S. G.; Xu, Z. K.; Chen, H.; Mak, C. L.; Wong, K. H.; Li, K. F.; Cheah, K. W. *J. Appl. Phys.* **2006**, *99*, 064103−064104.
(36) Souza, A. E.; Santos, G. T. A.; Barra, B. C.; Macedo, W. D.; Teixeira, S. R.; Santos, C. M.; Senos, A. M. O. R.; Amaral, L.; Longo, E. *Cryst. Growth Des.* **2012**, *12*, 5671−5679.
(37) Moreira, M. r. L. c.; Buzolin, P. G. C.; Longo, V. M.; Nicoleti, N. H.; Sambrano, J. R.; Li, M. S.; Varela, J. A.; Longo, E. *J. Phys. Chem. A* **2011**, *115*, 4482−4490.
(38) Longo, E.; Orhan, E.; Pontes, F. M.; Pinheiro, C. D.; Leite, E. R.; Varela, J. A.; Pizani, P. S.; Boschi, T. M.; Lanciotti, F., Jr.; Beltrán, A.; Andrés, J. *Phys. Rev. B* **2004**, *69*, 125115.
(39) Beaury, O.; Faucher, M.; Caro, P. *Mater. Res. Bull.* **1978**, *13*, 175−185.
(40) Diot, N.; Benard-Rocherulle, P.; Marchand, R. *Powder Diffr.* **2000**, *15*, 220−226.
(41) Blasse, G. *Prog. Solid State Chem.* **1988**, *18*, 79−171.
(42) Lakshminarayana, G.; Qiu, J. *J. Alloys Compd.* **2009**, *476*, 720−727.
(43) Lakshminarayana, G.; Qiu, J.; Brik, M. G.; Kityk, I. V. *J. Phys.: Condens. Matter* **2008**, *20*, 335106.
(44) Blasse, G.; Grabmaier, B. C. *Luminescent Materials*; Springer-Verlag: Berlin, Germany, 1994.